

## Energy-loss straggling of helium projectiles at low kinetic energies: Deconvolution of concentration depth profiles of inorganic salt solutes in aqueous solutions

Gunther Andersson,<sup>1,2,\*</sup> Harald Morgner,<sup>2</sup> and Hartwig Pohl<sup>2</sup>

<sup>1</sup>*Flinders University, Department of Science and Engineering, School of Chemistry, Physics and Earth Science, GPO Box, 5001 Adelaide, Australia*

<sup>2</sup>*Wilhelm-Ostwald-Institute for Physical and Theoretical Chemistry, Leipzig University, Linnestrasse 3, 04103 Leipzig, Germany*

(Received 10 December 2007; revised manuscript received 21 July 2008; published 19 September 2008)

Neutral impact collision ion scattering spectroscopy allows to determine concentration depth profiles. The method makes use of the energy loss of projectiles passing through matter to gain the depth information. The energy losses of the projectiles obey a statistical distribution, the energy-loss straggling. The energy-loss spectra are mainly given by the energy-loss straggling and the concentration depth profiles. Knowing the energy-loss straggling quantitatively makes it possible to deconvolute the energy-loss spectra. Here we use the Poisson distribution to describe the energy-loss straggling. The Poisson distribution and a previously developed method are used to deconvolute the energy-loss spectra of iodide of aqueous LiI solutions with concentrations between 5 and 7.2*m*. The iodide concentration depth profiles of these highly concentrated solutions are monotonous and do not show a local maximum near the surface.

DOI: 10.1103/PhysRevA.78.032904

PACS number(s): 34.50.Bw, 68.03.Hj

### I. INTRODUCTION

For a few decades ion scattering spectroscopy is used to determine concentration depth profiles and a lot of progress has been gained in improving the depth resolution. In most cases high- or medium-energy methods such as Rutherford backscattering (RBS) [1,2] and medium-energy ion scattering (MEIS) [3] are used. Neutral impact collision ion scattering spectroscopy (NICISS) using low-energy helium projectiles can be used to determine concentration depth profiles in the surface near region with a depth resolution of a few Å of samples which do not have long-range order such as polymers or liquids [4].

Ion scattering techniques using low-energy projectiles have to be used in vacuum. Thus the research of liquid surfaces seemed to be restricted to solvents with low vapor pressure such as formamide, 3-hydroxypropionitrile, or glycerol. As a consequence, water as the most important solvent of all but with a high vapor pressure has not been studied with ion-scattering methods until recently [5]. In Ref. [5] it was shown which measures make NICISS investigations of aqueous surfaces possible. The problems that have to be overcome are twofold. Firstly, the aqueous targets have to be handled in vacuum. Secondly, the influence of the gas phase on the spectra has to be quantified. The latter problem addresses amongst others the quantification of the energy-loss straggling of particles passing through matter.

The depth information in an ion scattering experiment is gained from the energy loss of the projectiles interacting with matter. Energetic ions and neutral atoms lose energy on their passage through matter by small angle scattering and electronic excitations. The slowing down process is accompanied by a spreading of the projectile energy which is due to the statistical fluctuations in the number of energy-loss processes and the distribution in the amount of energy loss per energy loss event. Thus a monoenergetic beam of par-

ticles will have a distribution of kinetic energies after passage through matter. The first moment of this distribution gives the mean energy loss and is called stopping power [6]. The nuclear stopping power refers to the slowing down by multiple small angle scattering events and the electronic stopping power refers to the electronic excitations. The second moment gives a measure of the width of the energy-loss distribution [6] and is called energy-loss straggling. The energy-loss straggling is divided into a nuclear part, which is due to the statistics of the small angle scattering events, and the electronic energy-loss straggling [7,8]. In a backscattering experiment there is an additional contribution to the energy distribution of the detected projectiles. The multiple small angle scattering events cause the blurring of the backscattering angle. The blurring of the backscattering angle itself also contributes to the broadening of the measured energy-loss distribution. This effect should be considered separately from the energy-loss straggling [5].

The energy resolution of a NICIS spectrum and hence the resolution of the concentration depth profiles is—apart from the resolution of the spectrometer—determined by the distribution of inelastic energy losses during the backscattering process and the energy-loss straggling of the projectiles. The distribution of inelastic energy losses during the backscattering process can be determined by gas phase experiments [9].

Energy-loss straggling of projectiles with high kinetic energies ( $\sim$ MeV) has been determined experimentally [10–13]. The distribution function of the energy losses has been calculated by solving the transport equation [14,15] or from binary collision theory [16]. For the calculation of the energy-loss distribution it is required to know the probability function of an energy loss. The function is known for high-energy particles [17]. If the maximum possible energy transfer in a single energy-loss process is not small compared to the total energy loss of a projectile, the energy-loss distribution will be asymmetric [12]. Asymmetric energy-loss distributions are also found in single collisions due to the large energy transfer to ionization of the inner shells [18].

Experimental results at low energies, however, are rare. The probability function of an energy loss is not known for

\*gunther.andersson@flinders.edu.au

low energies and thus the energy-loss distribution cannot be calculated following the approach of Landau and Vavilov [14,15]. Recently, measurements at surfaces of aqueous solutions of the surfactant  $\text{Bu}_4\text{NI}$  could be used to develop a procedure to determine the energy-loss straggling at low kinetic energies [5]. Comparing spectra of aqueous solutions at different temperatures and thus different vapor pressures, the distribution of probabilities have been determined that a helium projectile suffers an energy loss after penetrating through a layer consisting of a known amount of matter. In this procedure the probabilities for energy loss have been considered as the fitting parameters. The advantage of this procedure is, that no assumptions about the shape of the probability distribution have to be made. The disadvantage is, that the probability distribution could be given only for a multiple of a particular mean energy loss, that was given by the—discrete—values of the vapor pressure of the investigated solutions, i.e., the chosen temperature of the solutions during the measurements. As a consequence, this procedure is an incremental mathematical procedure making complicated practical applications such as the deconvolution of the spectra.

In a recent publication Pezzi *et al.* have shown that the energy-loss scattering in a medium-energy scattering (MEIS) experiment can be separated in a statistical contribution and the distribution of possible energy losses in the collisions [19]. They showed that the energy-loss straggling can be described by the sum of products of a function describing the probability for the occurrence of energy losses with a function describing the distribution of energy losses [19]. The probability is described by the Poisson statistics while the second function describes the energy-loss distribution after the number of scattering events considered with the respective Poisson coefficient.

In this paper we will use a similar but simplified approach to describe the energy-loss straggling. The first purpose of this paper is to develop a practical method for describing the energy-loss straggling at low kinetic energies and to show how this method can be applied to correct the energy-loss spectra for the energy-loss straggling. We will use here a Poisson distribution to account for the statistical nature of the energy-loss processes. We will use a single and fixed energy loss to describe the energy loss in a scattering event and thus use for the second function in the model of Pezzi *et al.* a  $\delta$  function. The second purpose of the paper is to show that the energy-loss distributions gained with both procedures—first procedure using the Poisson distribution, second procedure treating the probabilities itself as fitting parameters—are used to deconvolute the energy-loss spectra of highly concentrated aqueous  $\text{LiI}$  solutions. The focus of this paper is not to reveal more details about the energy-loss processes and the energy-loss straggling. We want to emphasize that it was the purpose of the first paper to find a model free description of the energy-loss straggling [4]. In this paper we will also describe how to handle the aqueous surface for the investigation by NICISS.

The investigation of aqueous inorganic salt solutions has attracted a lot of interest in the past years. Simulations stimulated the discussion whether or not polarizable inorganic ions such as iodide or bromide are enriched in the outermost layer

of aqueous solutions in spite of the surface excess of the respective salts being negative [20,21]. Recently Hemminger *et al.* showed that it is possible to investigate saturated aqueous solutions at low temperatures with x-ray photoelectron spectroscopy (XPS) [22,23], a technique also carried out in vacuum. Unfortunately, they were not able to show quantitative concentration depth profiles but concluded, that in saturated aqueous  $\text{KBr}$  and  $\text{KI}$  solutions the concentration of bromide and iodide, respectively, in the outermost layer is significant higher than that of potassium at the surface and also higher than that of the halide bulk concentration.

## II. EXPERIMENTAL

The method NICISS and the setup are described in detail in Ref. [24]. The target is bombarded with a pulsed beam of inert gas ions—mostly helium ions—with a kinetic energy of several keV. The energy of the projectiles backscattered from the atoms in the target is determined by their time-of-flight (TOF) from the target to the detector. The scattering angle used is  $168^\circ$  and the length of the TOF path is about 1.24 m. In all experiments shown here the target was oriented with the surface normal parallel to the direction to the detector. The time resolution can be estimated from the photon peak in the spectra and is 10 ns for the experiments shown here. The projectiles lose energy during the backscattering process and the energy transfer depends on the mass of the target atom. Additionally, the projectiles lose energy on their trajectory through the bulk due to small angle scattering of the projectile and electronic excitations of the molecules that constitute the target. The magnitude is proportional to the depth of the target atom. The depth that can be investigated by this method is limited by the blurring of the scattering angle due to multiple small angle scattering events. At an energy of 5 keV the maximum depth which can be investigated is about 300 Å. The dose of the He ions in a typical NICISS experiment investigating liquid surfaces is about  $10^{10}$  ions/cm<sup>2</sup>. Thus damage of the surface and the influence of the impinging ions on the surface structure can be neglected.

The method to create the liquid surface in the vacuum is described in detail in Ref. [24]. A reservoir in the vacuum chamber is filled with the liquid. A disk is immersed into the liquid and is rotated by a motor. As a result a thin lamella of the liquid develops on the disk. Due to the high vapor pressure of water, the target as described above cannot be used to investigate aqueous surfaces but has to be modified. For the investigation of aqueous surfaces, the target is placed in a closed housing with a small aperture in front of the disk. The ion beam analysis is carried out through the aperture as it is shown in Fig. 1. The diameter of the aperture was chosen as 1.0 mm. A second aperture with a diameter of 0.8 mm is mounted in front of the housing towards the ion source in order to shape the ion beam. The second aperture shall prevent the ion beam from hitting the aperture in front of the disk. This could not be fully avoided in all cases. The influence on the spectra is discussed in detail in Ref. [5].

The function of the housing with the aperture is twofold. First, due to the aperture the vacuum chamber is differen-

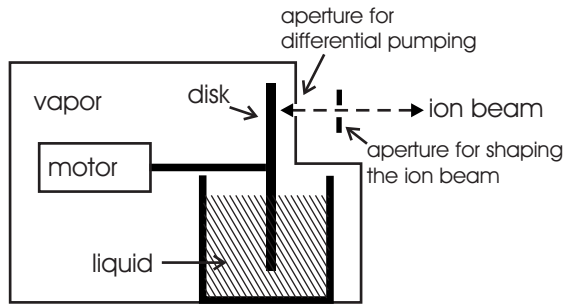


FIG. 1. Schematic of the target for the preparation and investigation of aqueous surfaces with NICISS.

tially pumped and the pressure in the housing is close to the vapor pressure of the liquid and thus helps to avoid boiling of the water. Secondly, the density of the gas phase adjacent to the target is reduced on the path of the projectiles. The second function strongly influences the spectra, since the depth resolution of the concentration depth profiles is limited by the straggling as described above. Thus it is essential to keep the amount of matter in the gas phase the projectiles have to pass through as small as possible by keeping the aperture and the distance between the aperture and the aqueous surface as small as possible.

The pressure on a line through the aperture is given by [23]

$$p(z') = (0.5p_0) \left( 1 - \frac{z'}{(1+z'^2)^{0.5}} \right), \quad (1)$$

where  $p_0$  is the pressure inside the housing,  $R$  is the radius of the aperture,  $z$  the distance to the center of the aperture, and  $z' = z/R$ . Negative values of  $z$  indicate the direction towards the region with the higher pressure. Equation (1) is based on the ideal gas theory for molecular flow conditions. Pressure profiles for two different radii of the aperture are shown in Fig. 2. The profiles show that both a small aperture and a small distance between the liquid surface and the aperture reduce the amount of gas phase the projectile has to pass through.

We reevaluate in this publication data on the aqueous solutions of  $0.01m$   $\text{Bu}_4\text{NI}$  and  $2.5m$   $\text{LiCl}$  which are published in Ref. [5]. Additionally we investigate solutions of  $\text{LiI}$  in

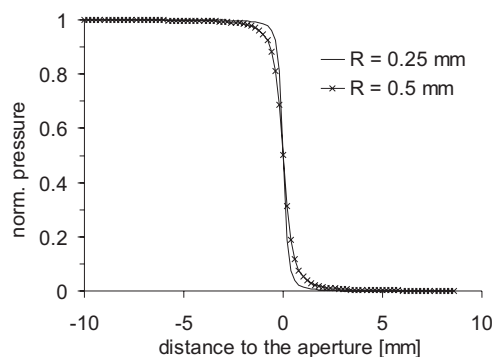


FIG. 2. Normalized pressure on the axis through the aperture. Negative values of  $z$  indicate the direction towards the housing.

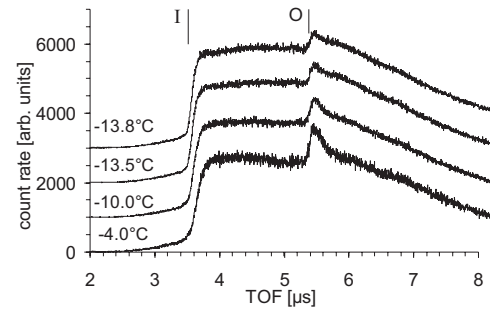


FIG. 3. TOF spectra of aqueous  $\text{LiI}$  solutions. The concentrations are  $-13.8^\circ\text{C}$ :  $7.2m$ ,  $-13.5^\circ\text{C}$ :  $6.7m$ ,  $-10^\circ\text{C}$ :  $6.6m$ ,  $-4^\circ\text{C}$ :  $5m$ . A vertical offset is added to the spectra for clarity.

water with concentrations between  $5$  and  $7.2m$ .  $\text{LiI}$  was purchased from Aldrich and the water used was deionized. The measurements were carried out with  $3$  keV helium ions. The detector efficiency was determined by measuring the spectra of a solution of  $\text{NaI}$  in formamide with a fixed bulk concentration at different primary energies. After correcting the spectra for the cross section, the detector efficiency can be determined by assuming that the concentration depth profile of the solute in the bulk is constant. The detector efficiency was taken into account in the data evaluation.

### III. RESULTS

#### A. Measurements

The NICIS spectra of the aqueous solution of  $0.01m$   $\text{Bu}_4\text{NI}$  and  $2.5m$   $\text{LiCl}$  are published in Ref. [5]. In Fig. 3 TOF spectra of the aqueous  $\text{LiI}$  solutions measured at different temperatures are shown and in Fig. 4 the respective energy-loss spectra. The vapor pressure of each solution is given in Table I. The vapor pressure is calculated from the thermodynamic data given in Ref. [25] at  $30^\circ\text{C}$ , taking into account the activity of  $\text{LiI}$ . The water activity at a given concentration as shown in Ref. [25] is almost constant over the temperature range of  $30$  to  $70^\circ\text{C}$ . Thus it may be assumed that the activity at the temperature used for the measurements here deviates only slightly from those at the temperatures used in Ref. [25]. The vapor pressure was

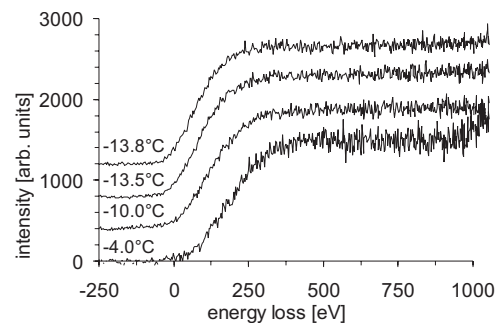


FIG. 4. Energy loss spectra of helium projectiles backscattered from iodide of the aqueous  $\text{LiI}$  solution. A vertical offset is added to the spectra for clarity. The temperatures and concentrations are the same as in Fig. 3

TABLE I. Vapor pressures of the solutions at the various temperatures calculated according to the activity of the LiI.

Temperature (°C)	Concentration (m)	Vapor pressure (mbar)
-13.8	7.2	1.0
-13.5	6.7	1.1
-10.0	6.1	1.7
-4.0	5.0	3.1

measured in Ref. [25] as pressure difference between the vapor pressure of pure water and that of the solutions.

Structures due to oxygen and iodide can be identified in the spectra. The onsets of the structures on the TOF scale are indicated with bars. The structures can be separated from the spectra as described in Ref. [26] and converted into the energy-loss scale. The energy loss is the difference between the energy of a projectile backscattered from a specific element being in the outermost layer and the measured energy of the projectile. The energy of a projectile backscattered from the outermost layer is gauged with gas phase spectra [9].

Projectiles backscattered from the liquid phase have to penetrate through the gas phase adjacent to the liquid phase. Due to the high vapor pressure of the water, the energy loss in the gas phase cannot be neglected. The energy-loss spectra of the projectiles backscattered from the constituents of the solute are shifted to greater energy loss and broadened. A detailed illustration of this phenomenon is given in Ref. [5]. The shape of the oxygen step is also discussed in detail in Ref. [5].

### B. Fitting the energy-loss distribution

The energy-loss spectrum of each element present in a target is given by (1) the concentration depth profile of the element, (2) the finite time length and the spread in energy due to the technique to produce the ion beam, (3) the energy loss and the energy-loss straggling of the projectiles penetrating through the surface near region up to the depth  $z$ , (4) the spread in inelastic energy losses during the backscattering event in the depth  $z$  and the spread in energy due to thermal vibrations of the target atom [27], (5) the energy loss and the energy-loss straggling of the projectiles penetrating through the surface near region from the depth  $z$  to the surface. Processes 2 and 4 are independent of the depth, from which the projectile is backscattered and are considered together in a single mathematical operation when fitting the spectra as will be described below. Typical values for the process 2 are 15 eV for 3 keV helium projectiles backscattered from iodide and 4 eV for 3 keV helium projectiles backscattered from oxygen. The process 4 is entirely represented by gas phase spectra. Typically, the FWHM of 3 keV helium projectiles backscattered from iodide is about 80 eV including the FWHM of about 15 eV for the spread in energy due to thermal vibrations [27]. The processes 3 and 5 are of the same nature and also considered together in the fitting process. Whether a process depends on the depth or not is the

only appropriate criterion in the decision which processes may be considered in the same mathematical operation. The influence of the processes 2 and 4 is given with the gas phase spectra and the energy loss straggling can be determined in a separate procedure.

The influences of processes 2 and 4 are considered with the function  $G_{\text{app}}$  and the energy loss straggling with the function  $F_{\text{stragg}}$ . The measured energy loss spectrum of an element  $I^{\text{exp}}(E_{\text{loss}})$  can be considered as a convolution of a hypothetical energy loss spectrum  $I(E_{\text{loss}})$ , that would be measured if the processes 2 and 4 could be neglected, with the gas phase spectrum of the respective element:

$$I^{\text{exp}}(E_{\text{loss}}) = \int_{-\infty}^{\infty} G_{\text{app}}(E_{\text{loss}} - E'_{\text{loss}}) I(E'_{\text{loss}}) dE'_{\text{loss}}. \quad (2)$$

The energy loss is the energy of the backscattered projectile less the energy of a projectile backscattered from the outermost layer. The latter quantity is determined from gas phase spectra as described above. The influence of the energy-loss straggling can also be mathematically described as convolution. One has to note, however, that the convolution function depends on the thickness of the layer that has to be penetrated by the projectile, i.e., on the depth of the atom from which the projectile is backscattered. The corresponding convolution function  $F_{\text{stragg}}(E_{\text{loss}}, z)$  depends on both, the energy loss  $E_{\text{loss}}$  and the depth  $z$ . The relation between the concentration depth profile  $c(z)$  and the hypothetical energy loss spectrum  $I(E_{\text{loss}})$  is

$$I(E_{\text{loss}}) = \int_0^{\infty} F_{\text{stragg}}(E_{\text{loss}}, z) c(z) dz. \quad (3)$$

It is also possible to combine Eqs. (2) and (3) and write them as

$$I^{\text{exp}}(E_{\text{loss}}) = \int_0^{\infty} H_{\text{app, stragg}}(E_{\text{loss}}, z) c(z) dz, \quad (4)$$

where

$$H_{\text{app, stragg}}(E_{\text{loss}}, z) = \int_{-\infty}^{\infty} G_{\text{app}}(E_{\text{loss}} - E'_{\text{loss}}) \times F_{\text{stragg}}(E'_{\text{loss}}, z) dE'_{\text{loss}}. \quad (5)$$

In Ref. [5]  $F_{\text{stragg}}$  was determined by considering the probabilities for the energy losses as fitting parameters. Here we use a different approach. We have conceived the occurrence of energy-loss events as independent of each other, which can be justified by their small cross section. This allows making use of the Poisson distribution. As additional simplification we assume that all collisions lead to the same amount of energy loss  $\Delta E_{\text{loss}}$ . This is less well justified, but comparison with experiment indicates that this approximation is acceptable.  $\Delta E_{\text{loss}}$  is a parameter that has to be determined by comparison with experiment. It turns out that the value of this parameter is not very critical. The number of scattering centers per area in the layer considered is named  $d$ . This quantity grows linearly with the layer thickness and thus can be considered as measure for the layer thickness.



The cross section for the event leading to energy loss  $\Delta E_{\text{loss}}$  shall be named  $\sigma$ . The Poisson distribution yields the probability that the projectile undergoes a number of  $k$  scattering events when passing through the considered layer

$$P_{\text{Poisson}}(k) = (\sigma d)^k \frac{\exp(-\sigma d)}{k!}. \quad (6)$$

The values of  $\sigma$  and  $d$  cannot be fitted independently but only their product. The distribution is normalized to give

$$\sum_{k=0}^{\infty} P_{\text{Poisson}}(k) = 1. \quad (7)$$

The mean energy loss is given by

$$\langle E_{\text{loss}} \rangle = \sigma d \Delta E_{\text{loss}}. \quad (8)$$

The individual energy loss is related to the number of collision events by

$$E_{\text{loss}} = k \Delta E_{\text{loss}}. \quad (9)$$

To any layer thickness  $d$  belongs a distribution of  $k$  and, thus, a distribution of energy losses. For the application it would be easier to have the distribution not as function of  $k$ , but of the energy loss. For this purpose we set

$$k = \frac{E_{\text{loss}}}{\Delta E_{\text{loss}}}. \quad (10)$$

This turns the integer number  $k$  into a continuous variable. We account for this by replacing the factorial  $k!$  by the Gamma function  $(k+1)$  which leads to

$$P_{\text{Poisson}}(E_{\text{loss}}) = (\sigma d)^{(E_{\text{loss}}/\Delta E_{\text{loss}})} \frac{\exp(-\sigma d)}{\Gamma\left(\frac{E_{\text{loss}}}{\Delta E_{\text{loss}}} + 1\right)}. \quad (11)$$

We note that the last operation is purely mathematical and does not affect the physical model of discrete energy loss events. The layer thickness is proportional to the parameter  $d$ . As in a NICISS experiment the projectile passes the layer twice (from the surface to the depth of the backscattering event and back to the surface) we write the Poisson distribution as

$$P_{\text{Poisson}}(E_{\text{loss}}) = (2\sigma d)^{(E_{\text{loss}}/\Delta E_{\text{loss}})} \frac{\exp(-2\sigma d)}{\Gamma\left(\frac{E_{\text{loss}}}{\Delta E_{\text{loss}}} + 1\right)}. \quad (12)$$

In Eq. (12) it is for sake of simplification neglected, that the path length of the outgoing trajectory is slightly longer than the depth due to the angle between the incoming ion beam and the surface normal. Secondly it is neglected that the energy loss on the outgoing trajectory is smaller than on the trajectory of the incoming projectiles due to the lower energy of the projectiles on the outgoing trajectory.

The fitting procedure comprises the convolution of the spectrum measured at a lower temperature with a Poisson distribution to fit the spectra measured at a higher temperature. At a fixed value of  $\Delta E$ , all possible combinations of the spectra were fitted. The parameter  $d$  is the only fitting param-

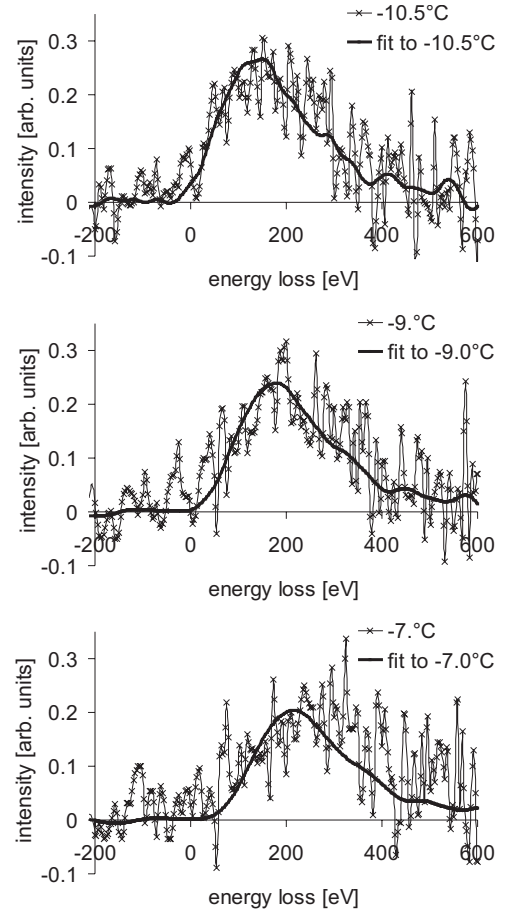


FIG. 5. Fit of the energy loss spectra of iodide in the aqueous  $\text{Bu}_4\text{NI}/\text{LiI}$  solutions as shown in Ref. [5]. The spectra are fitted by convoluting a spectrum measured at a lower temperature with a Poisson distribution. The fitting parameter is the number of energy loss events which are shown for all fits in Fig. 7. The convoluted spectrum is in all cases the  $-13.2^\circ\text{C}$  spectrum. The average energy loss per energy loss event used to calculate the Poisson distribution is 6 eV.

eter while  $\sigma$  is set equal to unity. Fits were carried out for  $\Delta E$  in the range of 3 to 9 eV. The justification for this range of  $\Delta E$  is that approximating the water molecules as spheres and taking into account the density of water, the number of water molecules per monolayer in the condensed phase is about  $0.9 \times 10^{15}/\text{cm}^2$ . Using the extrapolated stopping power from Ref. [28] the average energy loss of a projectile passing by an oxygen atom is about 5.5 eV and by a single water molecule about 8.3 eV. The energy loss passing by a single hydrogen atom is small and can be neglected in reasoning the chosen range of  $\Delta E$ .

A few results are shown in Fig. 5 for  $\Delta E=6$  eV. Fitting the data it seems to be possible to optimize also the value of  $\Delta E$ . However, it turns out that the quality of the fit on the data shown in Ref. [5] does not depend strongly on  $\Delta E$ .

In Fig. 6 some energy-loss distributions for  $\Delta E=6$  eV are shown. It can be seen that the shape of the distributions changes from asymmetric to symmetric. It must be noted that for a fixed energy loss the shape of the Poisson distribution becomes more asymmetric as larger  $\Delta E$  is chosen. In Fig. 7

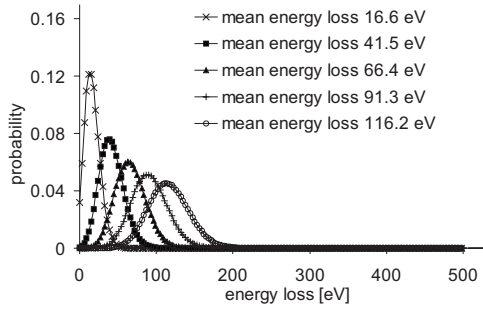


FIG. 6. Poisson distributions representing energy loss distributions for different mean energy losses. The average energy loss per energy loss event used to calculate the Poisson distribution is 6 eV.

the number of energy-loss events for different values of  $\Delta E$  (3, 6, and 9 eV) are shown as a function of the pressure difference in the main chamber during the measurements. The average number of energy-loss events depends linearly on the pressure difference. Taking the energy loss per event into account, we find a slope of  $56.7 \pm 3.4$  eV/ $10^{-4}$  mbar (3 eV/event),  $59.4 \pm 2.5$  eV/ $10^{-4}$  mbar (6 eV/event), and  $59.4 \pm 2.1$  eV/ $10^{-4}$  mbar (9 eV/event).

We have considered in the data evaluation shown here the trajectories of the projectiles as straight lines. However, the blurring of the scattering angle due to multiple small angle scattering events causes broadening of the energy distribution. The assumptions of straight trajectories breaks down when the broadening of the energy distribution due to the blurring of the scattering angle becomes comparable to the energy-loss straggling. In Fig. 8 the fullwidth at half maximum (FWHM) of the Poisson distributions is shown as well as the FWHM of the energy distribution caused by the blurring of the scattering angle as published in Ref. [5]. Figure 8 shows that the influence of the blurring of the scattering angle on the broadening of the energy distribution is much smaller than the influence of the energy loss straggling and supports the assumption of straight trajectories for the energy loss range considered here.

The data of the LiI solutions cannot be used to prove, whether or not the Poisson distribution is suitable to describe the energy-loss distribution. The reason is that these spectra show only a rising edge and not a falling edge as the spectra of the Bu<sub>4</sub>NI/LiCl solution published in Ref. [5] do show.

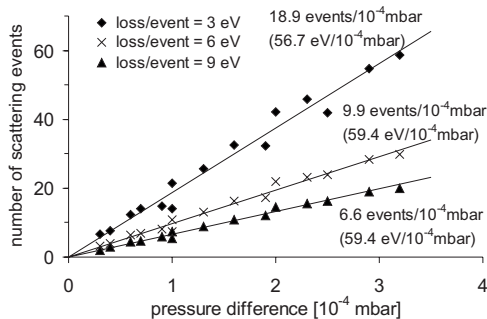


FIG. 7. The number of energy loss events for different mean energy losses as a function of the differences in vapor pressure as determined from fitting the energy loss spectra.

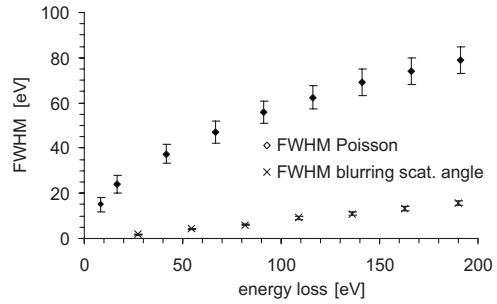


FIG. 8. FWHM of the Poisson distributions as shown in Fig. 6 as function of the mean energy loss. Additionally the FWHM of the energy distribution caused by the blurring of the scattering angle as published in Ref. [5] are shown.

### C. Deconvolution

The knowledge of the energy-loss distribution makes possible a further important step in the data evaluation. The energy-loss distribution as described above can be used to deconvolute the iodide spectra. For the deconvolution, the distribution of inelastic energy losses of the projectiles during the backscattering process has to be known as well as the distribution of kinetic energies of the primary ions. The distribution, taking into account both single distributions, is measured by gas phase experiments [9].

Further, the zero mark of the depth scale has to be gauged. This is done with the following procedure. (1) In the case of using the Poisson distribution to describe the energy-loss distribution, we treat the spectra of the aqueous LiI solution in the same way as the Bu<sub>4</sub>NI spectra in the previous section. (2) In the case of using the method as described in Ref. [5] we convolute several times a spectrum measured at a lower temperature with the energy-loss distribution for the mean energy loss of 8.3 eV to fit a spectrum measured at a higher temperature. The only fitting parameter here is the number of convolutions. The shift of the spectra as a function of the pressure difference is given in Fig. 9. The data can be fitted accurately with a straight line through the origin with a slope

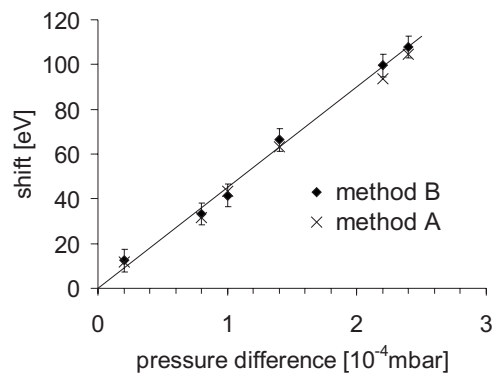


FIG. 9. Shift of the energy-loss spectra as a function of the pressure difference in the main chamber. The shift was determined by fitting a spectrum measured at a lower temperature by convoluting a spectrum measured at a higher temperature. Both the Poisson distribution as determined in this paper (method A) and the procedure described in Ref. [5] (method B) have been used.

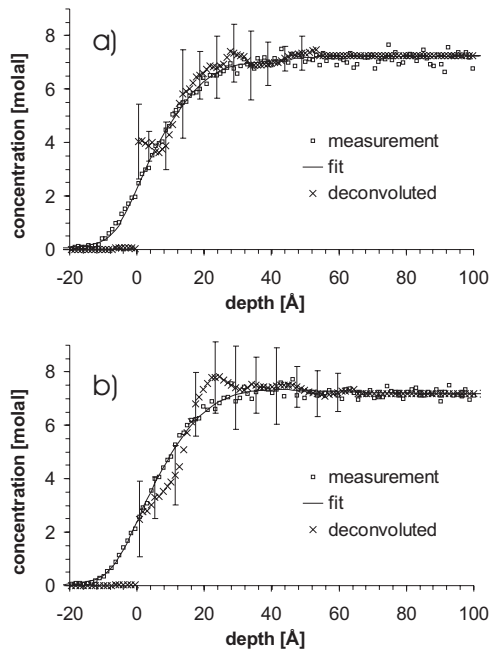


FIG. 10. Concentration depth profiles of iodide of an aqueous 7.2m LiI solution determined by deconvolution of the energy-loss spectrum using (a) a Poisson distribution as energy-loss distribution and (b) the procedure according to Ref. [5]. In Ref. [5] the energy-loss distribution is determined by considering the probabilities in the energy distribution of the projectiles penetrating through a thin gas phase layer as the fitting parameters thus not making use of a functional description of the energy-loss distribution.

of  $45.0 \pm 1.5$  eV/ $10^{-4}$  mbar. In this procedure we assume that the shape of the concentration depth profiles of the iodide in the surface near area of the aqueous LiI solutions does not change significantly over the concentration range of 5 to 7.2m and the temperature range of  $-13.2$  °C to  $-4$  °C. From the slope of the data shown in Fig. 9 we can read the offset of the zero mark of the depth scale with respect to the position of the maximum in the gas phase spectra.

The deconvolution of the iodide energy loss spectra was carried out with an algorithm as described in Ref. [4]. The deconvolution of the spectrum of the 7.2m solution measured at  $-13.8$  °C is shown in Fig. 10(a) using the Poisson distribution and in Fig. 10(b) using the method in Ref. [5] to describe the energy-loss distribution. The deconvoluted concentration depth profile differ a little in their slope but show both a monotonic increase of the iodide concentration from the surface to the bulk.

#### IV. DISCUSSION

We have reconsidered NICIS spectra of aqueous solutions of  $\text{Bu}_4\text{NI}$  and  $\text{LiCl}$ . We use the Poisson distribution to describe the probability distribution of energy losses with the product of the depth and the cross section as the expectation value for the number of energy-loss events. Both methods developed to describe the energy-loss straggling are used to deconvolute aqueous LiI solutions and to determine the concentration depth profiles of iodide.

In Ref. [5] we used a different method to determine the energy-loss distribution and it is worth to compare the results of both methods. The main difference is in the shape of the energy-loss distributions: the Poisson distribution used here is less asymmetric than the distribution determined with the method shown in Ref. [5]. However, the fit results are very similar. It might be possible that the current data basis with the low count rate of the spectra does not allow to judge whether or not either of the methods should be preferred. The Poisson distribution is superior from a practical point of view while the method described in Ref. [5] does not limit the variation of the shape by using a particular mathematical function. Most important is that the deconvolution of the iodide spectrum of the aqueous LiI solution yields similar results. In both cases we find a monotonous increasing concentration depth profile and a depletion of the iodide in the surface near region. This means that the question, which of the procedures to determine the energy loss distributions should be preferred, does not affect the main result of the investigation of the aqueous LiI solution.

Our finding that there is no local maximum at the surface in the iodide concentration depth profile is different to the results published by Ghosal *et al.* in Ref. [22] showing an enhanced concentration of iodide and bromide at the surface of saturated aqueous KBr and KI solutions. Although the concentrations of the solutions investigated here are lower than that investigated in Ref. [22] it is not likely that this is the reason for the differences since computer simulations show that the enhanced concentration of inorganic polarizable ions at the surface decreases with increasing concentration Ref. [29].

Different to Pezzi *et al.* [19] we have used a  $\delta$  function to describe the energy-loss distribution after a fixed number of scattering events. The energy-loss distribution we use here is determined solely by the Poisson statistics for the probability that an energy-loss event occurs. Certainly, it would be worse to determine the energy-loss distribution after a fixed number of scattering events. This could be achieved either by theoretical calculations or by fitting this distribution from energy-loss experiments. However, the experiments shown here would not allow either to prove a theoretical calculation or fitting from the experimental data. For either of these options an improvement in the statistics of the data acquisition has to be gained.

#### V. CONCLUSION AND OUTLOOK

We developed a second method to deconvolute the energy-loss spectra of helium projectiles by fitting the energy-loss straggling of the projectiles when passing through water vapor with Poisson distributions. The shape of the energy-loss distribution using the Poisson distribution is less asymmetric than the previously published. With the current data basis it is not possible to decide whether or not one of the methods should be preferred.

We determined concentration depth profiles of iodide in 5 to 7.2m LiI solutions. The energy-loss distributions have

been used to deconvolute the measured spectra. We find a monotonic increasing concentration depth profile without an enhanced concentration in the outermost layer, which is different to the results published by Ghosal *et al.* in Ref. [22].

#### ACKNOWLEDGMENTS

We want to acknowledge the support of the German Science Foundation (DFG, Grant No. Mo 288/34).

- 
- [1] K. Kimura, S. Joumori, Y. Oota, K. Nakajima, and M. Suzuki, Nucl. Instrum. Methods Phys. Res. B **219-220**, 351 (2004).
- [2] S. K. Srivastava, D. Plachke, A. Szökefalvi-Nagy, J. Major, and H. Carstanjen, Nucl. Instrum. Methods Phys. Res. B **219-220**, 364 (2004).
- [3] T. Gustafsson, H. C. Lu, B. W. Busch, W. H. Schulte, and E. Garfunkel, Nucl. Instrum. Methods Phys. Res. B **183**, 146 (2001).
- [4] G. Andersson and H. Morgner, Surf. Sci. **445**, 89 (2000).
- [5] G. Andersson, Phys. Rev. A **75**, 032901 (2007).
- [6] E. Kührt and R. Wedell, Phys. Lett. **96A**, 347 (1983).
- [7] E. Szilágyi, Nucl. Instrum. Methods Phys. Res. B **161-163**, 37 (2000).
- [8] M. A. Briere and J. P. Biersack, Nucl. Instrum. Methods Phys. Res. B **64**, 693 (1992).
- [9] G. Andersson, H. Morgner, and K.-D. Schulze, Nucl. Instrum. Methods Phys. Res. B **190**, 222 (2002).
- [10] D. L. Mason, R. Prior, and A. R. Quinton, Nucl. Instrum. Methods **45**, 41 (1966).
- [11] K. W. Kemper, D. Haynes, and N. Fletcher, Nucl. Instrum. Methods **88**, 289 (1970).
- [12] B. Effen, D. Hahn, D. Hilscher, and G. Wüstefeld, Nucl. Instrum. Methods **129**, 219 (1977).
- [13] H. Bichsel, Phys. Rev. A **9**, 571 (1974).
- [14] L. D. Landau, J. Phys. (USSR) **8**, 201 (1944); in *L. D. Landau, Collected Papers*, edited by D. ter Haar (Pergamon Press, Oxford, 1965), p. 471.
- [15] P. V. Vavilov, Sov. Phys. JETP **5**, 749 (1957).
- [16] P. Sigmund and A. Shinner, Eur. Phys. J. D **23**, 201 (2003).
- [17] M. S. Livingston and H. Bethe, Rev. Mod. Phys. **9**, 245 (1937).
- [18] P. L. Grande, A. Hentz, R. P. Pezzi, I. J. R. Baumvol, and G. Schiwietz, Mat. Fys. Medd. K. Dan. Vidensk. Selsk. **52**, 151 (2006).
- [19] R. P. Pezzi, P. L. Grande, M. Cople, G. Schiewitz, C. Krug, and I. J. R. Baumvol, Surf. Sci. **601**, 5559 (2007).
- [20] B. C. Garrett, Science **303**, 1146 (2004).
- [21] P. Jungwirth and D. Tobias, Chem. Rev. (Washington, D.C.) **106**, 1259 (2006).
- [22] S. Ghosal, J. C. Hemminger, H. Bluhm, B. S. Mun, E. L. D. Hebenstreit, G. Ketteler, D. F. Ogletree, F. G. Requejo, and M. Salmeron, Science **307**, 563 (2005).
- [23] D. F. Ogletree, H. Bluhm, G. Lebedev, C. S. Fadley, Z. Hussain, and M. Salmeron, Rev. Sci. Instrum. **73**, 3872 (2002).
- [24] G. Andersson and H. Morgner, Surf. Sci. **405**, 138 (1998).
- [25] K. R. Patil, A. D. Tripathi, G. Pathak, and S. S. Katti, J. Chem. Eng. Data **35**, 166 (1990).
- [26] G. Andersson, T. Krebs, and H. Morgner, Phys. Chem. Chem. Phys. **7**, 136 (2005).
- [27] E. Hulpke, Surf. Sci. **52**, 615 (1975).
- [28] J. Ziegler, *Helium Stopping Powers and Ranges in All Elements* (Pergamon Press, Oxford, 1977).
- [29] P. B. Petersen, R. J. Saykally, M. Mucha, and P. Jungwirth, J. Phys. Chem. B **109**, 10915 (2005).